40th Fluid Dynamics Conference and Exhibit
28 June - 1 July 2010, Chicago, Illinois

AIAA 2010-4462

Experimental Study of a Rapidly Pitched Flat Plate at Low Reynolds Number

Yeon Sik Baik[1] , Hikaru Aono[2], Jonathan M. Rausch[3], Luis P. Bernal[4] , and Wei Shyy[5]
University of Michigan, Ann Arbor, MI

Michael V. Ol[6]
Air Force Research Lab, Wright-Patterson AFB

Abstract

We report the results of an experimental and numerical study of a rapidly pitched flat plate airfoil at *Re* = 5,000. The flat plate airfoil undergoes a 90° pitch-ramp maneuver about the quarter chord point with smooth starting and stopping transients. Reduced frequencies, $k = \dot{\theta}c/2U_\infty$, of 0.2 and 1.0 are investigated with dye flow visualization and 2D PIV. The main objective of the research is to determine the leading edge vortex (LEV) and trailing edge vortex (TEV) dynamics, and force generation during the high pitch-rate maneuver. The LEV and TEV formation and evolution are characterized in terms of vortex core location and circulation. The force coefficients are computed using the PIV data and are compared to recent direct force measurements and numerical simulations. Large force coefficients well beyond the steady flow values are measured during the motion. It is shown that as reduced frequency is increased large aerodynamic forces are produced, before formation of the LEV. Vortex topology also changes. For the low reduced frequency the flow topology is characterized by a strong LEV vortex and relatively weak TEV. For the high reduced frequency the TEV forms first and LEV formation is delayed until after completion of the motion.

I. Introduction

The study of unsteady aerodynamics of pitching wings is of interest for possible application to Micro Air Vehicle (MAV) design. MAVs are often characterized by low *Re* and the recent monograph by Shyy *et al.* [1] provides a detailed review of the subject. Transient motions enable birds and insects to perform rapid maneuvers. For example birds and insects are able to respond to gusts with flow speeds comparable to their flight speed. Similarly perching is another intriguing maneuver which is often observed from birds; birds tend to rotate their wings normal to the free stream and flap at high frequency in order to hover for a short period of time during landing. A typical perching maneuver produces massive unsteady separation of the flow about the wing and formation of large leading edge vortical structures. The formation of leading edge vortices are prominent features in flapping wing aerodynamics [2] and are believed to be critical to force generation [3-5]. Additionally, the formation of a leading edge vortex is a feature also found in helicopter blade aerodynamics, which produces the high lift coefficients associated with dynamic stall [6]. The flow field produced by these airfoil or wing motions, whether they are periodic or transient, must be understood well for application to MAV design.

1. Graduate Research Assistant, University of Michigan, Department of Aerospace Engineering, yeonb@umich.edu
2. Post Doctoral Research Fellow, University of Michigan, Department of Aerospace Engineering, aonoh@umich.edu
3. Graduate Research Assistant, University of Michigan, Department of Aerospace Engineering, rauschjm@umich.edu
4. Associate Professor, University of Michigan, Department of Aerospace Engineering, lpb@umich.edu
5. Clarence L. "Kelly" Johnson Collegiate Professor and Chair, University of Michigan, Department of Aerospace Engineering, weishyy@umich.edu
6. Aerospace Engineer, Air Vehicles Directorate, Wright-Patterson AFB, Michael.Ol@wpafb.af.mil

Studies of airfoils and wings undergoing rapid pitch motion to a high angle of attack were motivated by application to highly maneuverable aircraft [7-11]. This research has shown that large force coefficients develop at high pitch rates, which can reach lift coefficient values of order 10 at reduced frequency k = 1.0 [8]. Flow visualization studies noted the similarities between the flow evolution in high pitch rate maneuvers and the phenomenon of dynamic stall [6] observed in oscillating airfoils and wings. A perching maneuver, as seen from birds, can be viewed as a similar problem characterized by rapid change in angle of attack due to the rotation of the wing [11,13]. A simplification used frequently in experimental and numerical studies is to neglect the translational motion of the wing. Dickinson *et al*. [3] performed a study of an impulsively translating wing at different fixed angles of attack and stressed the fact that the LEV generation due to the unsteady motion is critical to lift generation. Ringuette *et al.* [12] performed an experiment of an impulsively translating flat plate with AR = 2 and 6 wings at 90° in order to investigate the development of wake vortices. Recently, Ol *et al.* [13] performed a series of flow visualization experiments on linear pitch ramp-hold-return cases. Their study included various pitch rates, pivot locations, aspect ratio, and pitch amplitude for a SD7003 airfoil and a flat plate with 2.5% thickness at Re = 10,000.

The current study explores similar parameter values used by Ol *et al.* [13]. The experiments are conducted at Re = 5,000 with angular amplitude of 90°. The kinematics is a linear pitch-ramp with smooth starting and stopping transients. These transients consist of a sinusoidal change of the pitch angle over 4.5 degrees where the pitch rate varies from zero to the desired pitch rate for the starting transient, and from the desired pitch rate to zero for the stopping transient. The pitch rate is varied to obtain reduced frequency $\left(k = {\dot{\theta}c}/{2U_\infty}\right)$ values of 0.2 and 1.0. Dye injection flow visualization along with 2D particle image velocimetry (PIV) is used to quantify the flowfield. The sectional lift and drag coefficient time history is computed using the "Flux Equation" as derived by Noca *et al.* [14]. Furthermore, the vortex identification methodology developed by Graftieaux *et al.* [15] is implemented to identify the vortex core and its boundaries. This technique is used to compute the leading edge vortex circulation and the results are compared with the vortex circulation values for the impulsively translating flat plate reported by Ringuette *et al.* [12].

II. Methodology

A. Experimental Setup

The experiments were conducted at the University of Michigan low-turbulence water channel facility. The test section is 2-by-2 feet and the free stream turbulence intensity is less than 1 %. The water channel free stream velocity can vary in the range 5 cm/s to 40 cm/s. The airfoil model is a 76-mm chord 6.25% thick stainless steel flat plate with rounded leading and trailing edges. The model is mounted vertically in the water channel test section less than 1 mm from the bottom glass wall. An endplate is installed just below the free surface minimize free surface effects and simulate 2D infinite aspect ratio wing. The airfoil pitching motion is produced by a rotary stage (Velmex B4872TS Rotary Table) and the associated computer control system (Velmex VXM-1-1 motor control). Figure 1 shows pictures of the water channel facility, motion rig and model installation.

Dye injection flow visualization was used for qualitative analysis. The dye flow visualization system consists of seven coplanar dye streams spaced 35 mm and introduced a half chord upstream of the leading

edge of the model at the mid-span plane. Two syringe pumps are used to introduce the dye stream at the same speed as the water channel flow speed in order to minimize disturbances produced by the wake of the dye injection system. The dye streams are held fixed and the airfoil is pitched within the width of the dye streams. The resulting streaklines capture flow direction and recirculation zones produced by the pitching motion of the flat plate.

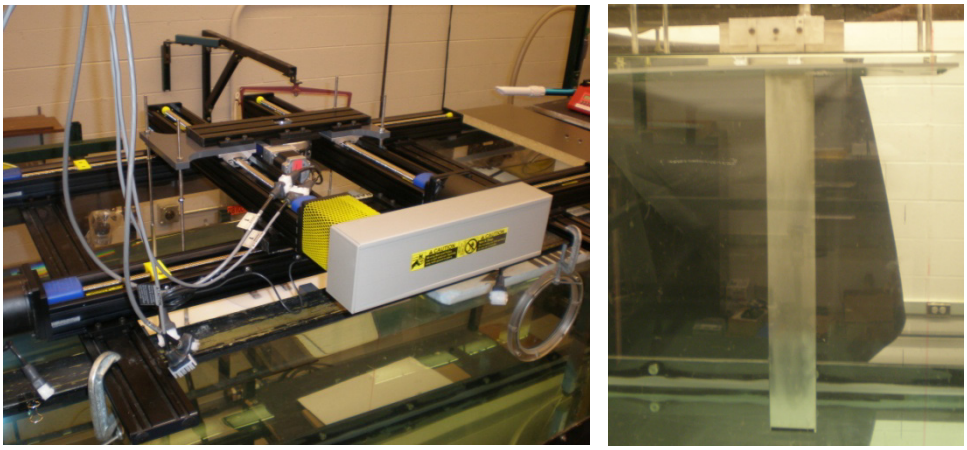

Figure 1. Water channel facility at the University of Michigan. Traverse motors with rotary stage (LEFT), and infinite AR flat plate with endplate mounted (RIGHT).

The 2D Particle image velocimetry (PIV) technique was used for quantitative flow analysis. The PIV system includes a double-pulsed Nd-YAG laser (Spectra Physics PIV 300), light sheet formation optics, two dual frame digital cameras (Cooke Corp. PCO.4000), computer image acquisition system and control electronics. The laser sheet was located at the mid-span plane and 50 image pairs were recorded at selected phases of the motion. For PIV image acquisition, the water channel was seeded with 3μm diameter Titanium Dioxide particles (Sigma-Aldrich). A small amount (8 drops in a 5,000 gallons total water channel volume) of a dispersant (DARVAN C-N, Vanderbilt) was used to produce a uniform distribution of particles and to help maintain the particles in suspension for long periods of time, typically on the order of several days. The cameras were installed underneath the water channel test section and were equipped with Nikon 105-mm Micro-Nikkor lenses to produce a magnification of approximately 11.5 pixels/mm. With this magnification the time between exposures was adjusted to produce a nominal particle displacement of 8 pixels at the free stream velocity for all cases. The PCO.4000 camera frame size is 4008 by 2672 pixels, which for the present magnification corresponds to a physical image size of 349 by 232 mm in the flow. A detailed description of dye injection flow visualization and PIV technique used in this paper can be found in Baik *et al.* [16]

B. Computational Setup

The governing equations are the incompressible, unsteady, three-dimensional Navier-Stokes equations with constant density and viscosity shown in Eq. (1) and (2),

$$\frac{\partial u_j}{\partial x_j} = 0, \tag{1}$$

$$\frac{\partial u_i}{\partial t} + \frac{\partial u_j u_i}{\partial x_j} = -\frac{1}{\rho_f}\frac{\partial p}{\partial x_i} + \mu\frac{\partial}{\partial x_j}\left(\frac{\partial u_i}{\partial x_j}\right), \quad (2)$$

where u_i is the velocity vector, x_i is the position vector, t is the time, p is the pressure, ρ_f is the fluid velocity, and μ the viscosity of the fluid. The Eqs (1) and (2) are solved with an in-house code [17,18] which is an unstructured, pressure-based finite-volume solver written in the LOCI-framework [19]. It employs implicit first or second order time stepping treats convection terms using the second order upwind-type scheme [17,20,21] , pressure and viscous terms using second order schemes. The system of equations resulting from the linearized momentum equations are handled with the symmetric Gauss-Seidel [22] solver which has relatively low memory requirements [23]. The pressure correction equation [17,24] is solved with the GMRES linear solver with Jacobi preconditions provided by PETSc [24]. The Loci framework is by design rule-based highly parallelizable, see Luke and George [19] for a more detailed discussion on rule-based software. The geometric conservation law, a necessary consideration in domains with moving boundaries, is satisfied [25,26]. The lump pitching motion is realized by rigid rotation of whole mesh.

Figure 2 shows computational grid of the flat plate. The distance from the plate to outer boundary is 50 chord lengths. Total number of cells is approximately 400,000, and the space of first grid from the flat plate is 0.15% chord length. Boundary condition for outer boundary is set to free stream velocity and density, and on flat plate no-slip condition is assigned. In current study, flow is assumed as laminar. The time step of 1×10^{-3} is utilized.

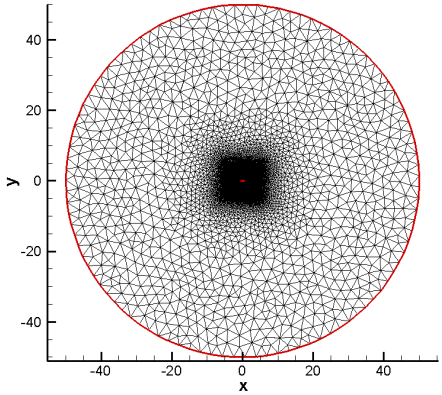

Figure 2. Schematic of computational grid.

III. Results

The kinematics considered in this paper is a linear pitch-ramp motion with smoothing. A sinusoid with 4.5° amplitude was used at the start and the end of the motion in order to suppress vibration induced by sudden start and stop motion. The pivot point is located at the quarter-chord. The initial angle of attack is set at 0° and the angular amplitude considered is 90°. The *Re*, based on chord of 76 mm, is held fixed at 5,000. Figure 3 illustrates the kinematics as a function of non-dimensional time.

The reduced frequency is the relevant non-dimensional parameter which is defined as $k = {}^{\dot{\theta}c}/_{2U_\infty}$. $\dot{\theta}$ is the angular velocity in rad/s, c is the chord, and U_∞ is the free stream velocity. The angular velocity is the only parameter that changes to produce different reduced frequency values. Current study explores k value of 0.2 and 1.0 which have approximate angular velocities of 20.2 °/s and 101°/s, respectively.

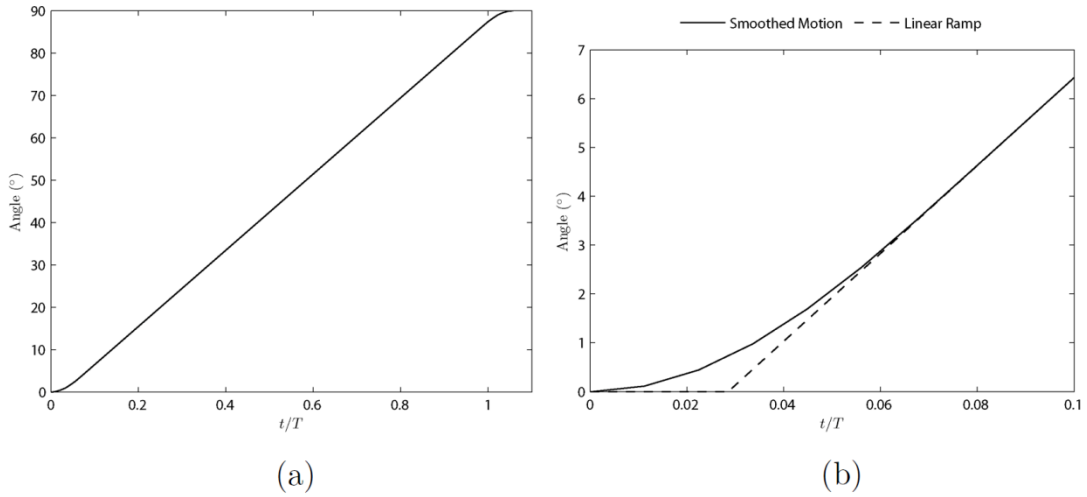

Figure 3. (a) Linear pitch-ramp motion with smoothing, (b) difference between smoothed function and ramp motion.

Dye injection flow visualization, PIV, and strain-gauge force balance are the experimental tools used to determine the flow field produced by the flat plate pitching motion.. Force measurements are of utmost interest in developing an engineering-tool for MAV design. At low Reynolds number the magnitude of the force is small which could results in significant resolution and signal-to-noise problems. In the current study, we measure the force on the flat plate airfoil from the measured velocity vector fields and time derivatives. Noca *et al.* [14] derived three formulations to compute the force acting on a body given an arbitrary control volume that encloses the body. In particular, the "Flux Equation" only requires a surface integral whereas the other two formulations require a volume integral over the control volume. The "Flux Equation" requires control surfaces, $S(t)$ and $S_b(t)$, where it denotes arbitrary control volume enclosing the body and body boundary, respectively. The "Flux Equation" and an illustration of control volumes are given by Figure 4.

$$\boldsymbol{F} = \oint_{S(t)} \hat{\boldsymbol{n}} \cdot \gamma_{\text{flux}}\, \mathrm{d}S - \oint_{S_b(t)} \hat{\boldsymbol{n}} \cdot (\boldsymbol{u} - \boldsymbol{u_s})\, \mathrm{d}S - \frac{\mathrm{d}}{\mathrm{d}t} \oint_{S_b(t)} \hat{\boldsymbol{n}} \cdot (\boldsymbol{ux})\, \mathrm{d}S$$

$$\gamma_{\text{flux}} = \frac{1}{2}u^2\boldsymbol{I} - \boldsymbol{uu} + \frac{1}{N-1}\big(\boldsymbol{\omega}(\boldsymbol{x}\times\boldsymbol{u}) - \boldsymbol{u}(\boldsymbol{x}\times\boldsymbol{\omega})\big)$$

$$-\frac{1}{N-1}\left[\left(\boldsymbol{x}\cdot\frac{\mathrm{d}\boldsymbol{u}}{\mathrm{d}t}\right)\boldsymbol{I} - \boldsymbol{x}\frac{\mathrm{d}\boldsymbol{u}}{\mathrm{d}t} + (N-1)\frac{\mathrm{d}\boldsymbol{u}}{\mathrm{d}t}\boldsymbol{x}\right] + \frac{1}{N-1}[\boldsymbol{x}\cdot(\boldsymbol{\nabla}\cdot\boldsymbol{T})\boldsymbol{I} - \boldsymbol{x}(\boldsymbol{\nabla}\cdot\boldsymbol{T})] + \boldsymbol{T}$$

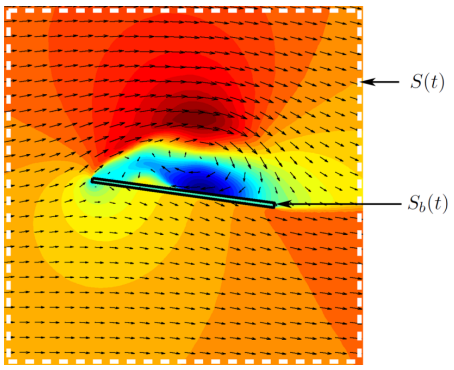

Figure 4. The "Flux Equation" and a schematic of the control surfaces.

$\hat{\boldsymbol{n}}$ is the unit normal 3-component vector, $\boldsymbol{u}$ is the 3-component velocity vector, $\boldsymbol{x}$ is the 3-component position vector, $\boldsymbol{I}$ is a unit matrix or identity matrix, $\boldsymbol{T}$ is the viscous tensor, and N is the dimension. The 2nd term in the "Flux Equation" is equal to zero since the body has no slip condition. The 3rd term also vanishes as the thickness of the airfoil is thin. Therefore, all that is needed is the information along the control volume that encloses the body to perform the surface integral. Compared to other formulations introduced, the "Flux Equation" circumvents the need for volume integrals including the velocity field near the body surface which are difficult to measure with PIV. The "Flux Equation" holds for a divergence free velocity vector fields.

The main focus of vortex dynamics in current study is the evolution of the LEV; the presence of the LEV core and the strength of LEV analyzed. Vortex identification method used by Graftieaux *et al*. [15] is implemented in identifying the LEV core locations and its boundary. The method is suitable for PIV measurement since it only requires well defined velocity vector fieldsf\. There are two criteria defined in this method: Γ_1 criterion which identifies the vortex core, and Γ_2 criterion which identifies the boundary of a vortex. Γ_1 and Γ_2 criteria are given by Eq. (3) and (4), respectively.

$$\Gamma_1(P) = \frac{1}{N}\sum_{i=1}^{N}\frac{(\overrightarrow{x_P}-\overrightarrow{x_i})\wedge\overrightarrow{u_i})\cdot\vec{k}}{\|\overrightarrow{x_P}-\overrightarrow{x_i}\|\cdot\|\overrightarrow{u_i}\|} \tag{3}$$

$$\Gamma_2(P) = \frac{1}{N}\sum_{i=1}^{N}\frac{\left((\overrightarrow{x_P}-\overrightarrow{x_i})\wedge(\overrightarrow{u_i}-\overrightarrow{u_p})\right)\cdot\vec{k}}{\|\overrightarrow{x_P}-\overrightarrow{x_i}\|\cdot\|(\overrightarrow{u_i}-\overrightarrow{u_p})\|} \tag{4}$$

P is any point on the flow field, $\vec{x}$ is the position vector, $\vec{u}$ is the velocity vector, $\vec{k}$ is the unit vector in the z-direction, and N is the total number of points in a control volume. The algorithm selects N number of points around a point P and computes Γ_1 and Γ_2. The maximum value of Γ_1 and Γ_2 is 1. Γ_2 criterion determines whether flow at point P is dominated by strain or rotation; if $|\Gamma_2|$ is less than $2/\pi$ it is strain dominated and if $|\Gamma_2|$ is greater than $2/\pi$ it is rotation dominated. It is possible to have a rotating flow with no definite vortex core but still have $|\Gamma_2|$ greater than $2/\pi$. While the theoretical threshold value of $|\Gamma_2|$ for rotation dominated flow is $2/\pi$, the method is weakly dependent on the distance between points and a characteristic length scale of the vortex. Graftieaux *et al*. [15] showed that the threshold value of $|\Gamma_2|$ stays within the range of 0.6 ~ 0.7 regardless of the ratio of characteristic lengths. The processed PIV data have a set distance between points of 16 pixels and $|\Gamma_2|$ threshold value was set at 0.65. A sample plot of vortex identification algorithm is shown in Figure 5.

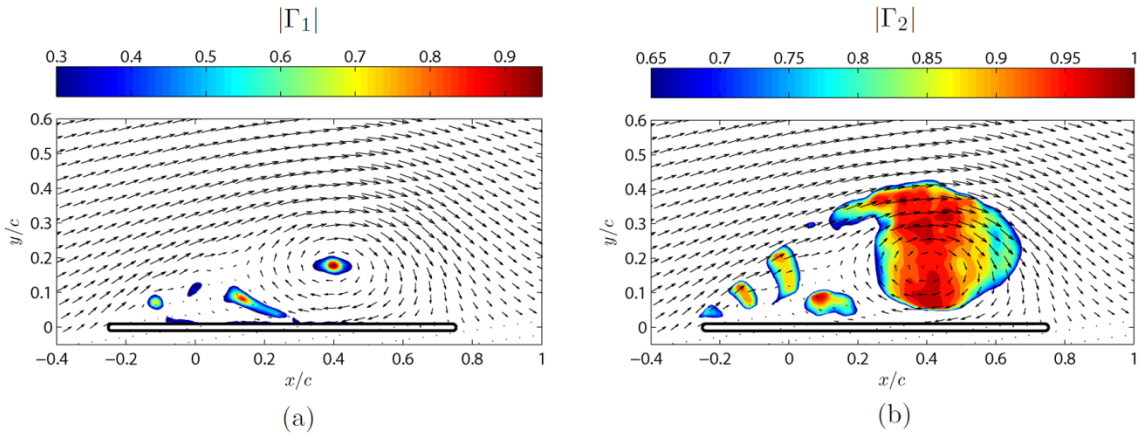

Figure 5. The velocity vectors with (a) contour of $|\Gamma_1|$, and (b) contour of $|\Gamma_2|$

A vortex core typically has a $|\Gamma_1|$ value greater than 0.9. Figure 5(a) is showing a vortex core at $x/c \approx 0.4$ which is in an excellent agreement with the velocity vectors. At $x/c \approx 0.15$, a $|\Gamma_1|$ value of 0.85 is recorded which indicates a possibility of secondary vortex formation. The boundary of the vortex core located $x/c \approx 0.4$ is shown in Figure 5(b). Notice that there are 3 distinct regions captured by the $|\Gamma_2|$ contours in the shear layer location. The locations of these regions are synchronous with the vortical structures found in instability of shear layer analysis. The flow is rotation dominated but does not have a definite vortex core. Once the boundary of the LEV is determined the circulation of this vortex can be computed from Eq. (5).

$$\Gamma = \iint \vec{\omega} \cdot \vec{n}\, dA = \sum_{i=1}^{N} \omega_{z_i} \tag{5}$$

Γ is the circulation which is not to be confused with the Γ_1 and Γ_2 criteria used in vortex identification algorithm. The enclosed area of the LEV found from $|\Gamma_2|$ criterion consists of N number of total points in the PIV grid and the integral simplifies to summation of all the vorticity with the normal in the in-plane direction.

A. Results: k = 0.20

A dye injection flow visualization in comparison with the PIV data for $k = 0.20$ case is shown in Figure 6. The PIV data were taken at every 9° between 0° and 90°. The vortex identification method proposed by Graftieaux *et al.* [15] was implemented; Γ_1 criterion identifies the vortex core location whereas Γ_2 criterion captures the boundary of a vortex. The threshold for Γ_1 was set at 0.9 and Γ_2 was set at 0.65. Overall, there is a good agreement between the flow visualization and the PIV data set. The von Karman vortex streets are observed in the wake at low angles of attack. The pitching motion persists for approximately 4.2 convective time, c/U_∞, thus the vortex streets disappear in downstream when the pitching maneuver is completed. Small vortical structures due to the Kelvin-Helmholtz instability in the shear layer are formed at the initial phase of rotation near the trailing edge. The leading edge vortex core starts to develop when the flat plate is at 36° and it continues to develop until the flat plate motion stops at 90°. A trailing edge vortex starts to develop at latter phases, and it is clear from Γ_1 criterion that two vortex cores exist at 81° and 90°. Around the LEV, small vortical structures are observed in the flow visualization as well as the PIV data set. The existence of these vortical structures is due to the instability in the shear layer caused by the leading edge of the flat plate [27]. There is a strong resemblance between the normalized vorticity contours and Γ_2 contours; the only observable difference between the two contours is that Γ_2 contours show von Karman vortex streets at low angles of attack. From this similarities, the circulation of a vortex computed using the boundary of Γ_2 criterion is expected to be similar to the circulation computed by Ringuette *et al.* [12] where a vorticity threshold was used to determine the vortex boundary. The LEV circulation using $|\Gamma_2|$ criterion is plotted in Figure 7.

The LEV circulation accumulates as the flat plate is rotated from 0° to 90°. The fastest growth rate is recorded approximately between 45° and 72°, and the normalized circulation value peaks at 2.35 as shown in Figure 7(a). A sudden decrease in LEV circulation past 72° suggests that the LEV is fully developed and the additional circulation at 81° and 90° is due to the formation of small vortical structures from the leading edge shear layer. Ringuette *et al.* [12] performed an impulsively translated flat plate with AR = 6 at *Re* = 3,000 and reported several non-dimensional LEV circulation values with respect to non-dimensional time. The non-dimensional time scale is similar to the one used in our current study which is tU_∞/c. t is the physical time, U_∞ is the free stream velocity, and c is the chord length. The only

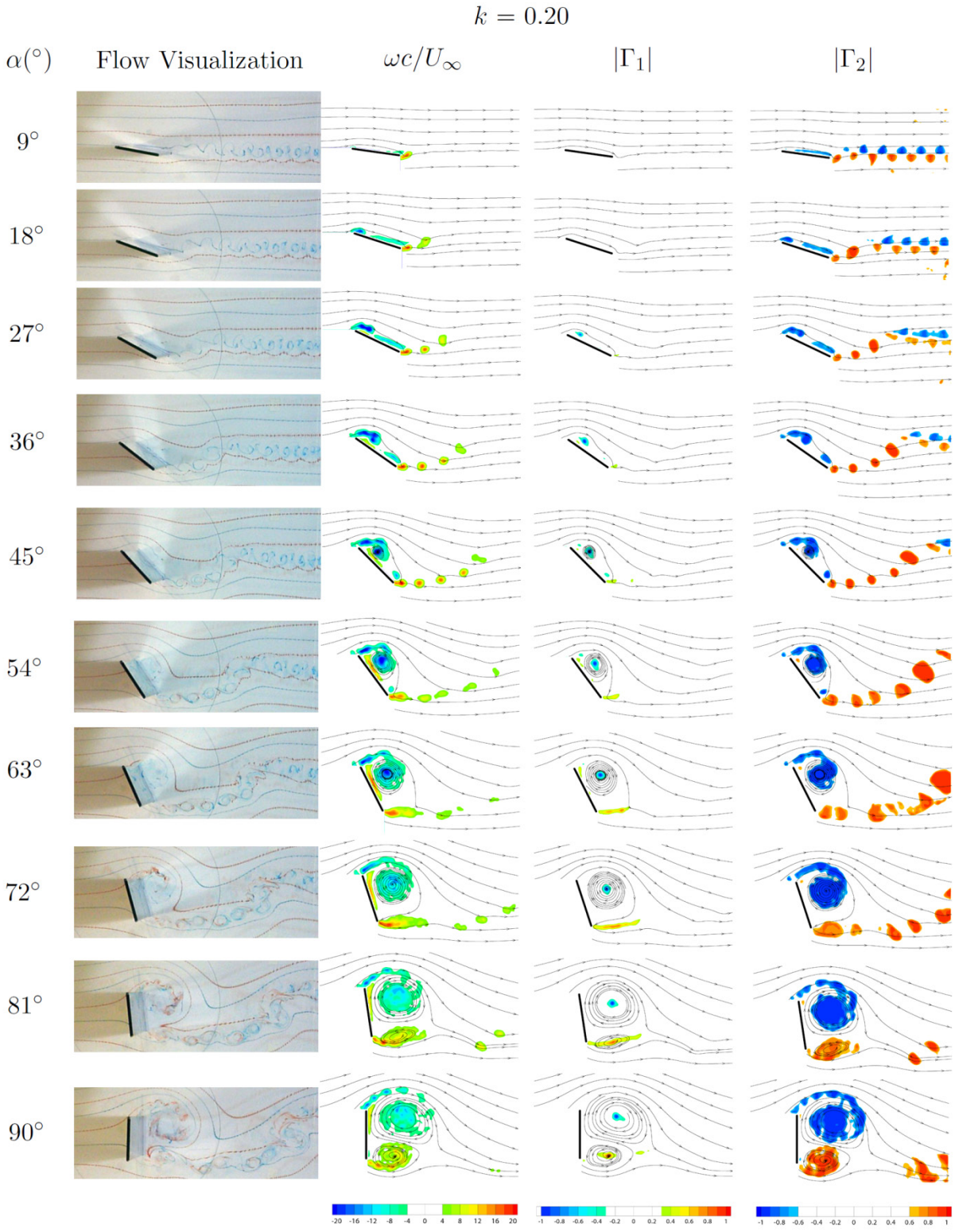

Figure 6. Summary of flow visualization, normalized vorticity, vortex core locations and size for k = 0.20 case.

difference in the definition is that the running mean velocity of the flat plate was used for impulsively translated flat plate instead of free stream velocity. Figure 7(b) compares the LEV circulation values obtained from the PIV data set and reported by Ringuette *et al.* [12] The initial build up of circulation differs since the impulsively started flat plate creates a shear layer at the edges with an effective angle of attack of 90°. On the other hand, the current study performs a rotation about the quarter-chord that does not create a strong shear layer in the leading edge until the geometric angle of attack is increased to a high value. Therefore, the circulation values obtained from both experiments agree better at latter tU_∞/c . The rotating flat plate is close to 90° at latter tU_∞/c and this may explain the similarity in the circulation value. The reported value of non-dimensional circulation for AR = 6 flat plate at 50% span location is approximately 5 at tU_∞/c = 4.2, which higher than the computed value of 4.5 for k = 0.2 case. Interestingly, the rate of change of the LEV circulation from tU_∞/c = 3.4 to 4.2 for both experiments seem to be in a good agreement.

The sectional lift and drag coefficients were computed by implementing "Flux Equation" proposed by Noca *et al.* [14] on the PIV data set. An independent force measurement was conducted for the same case using a force balance at the Air Force Research Laboratory (AFRL) [28]. In addition, the force coefficient correlations reported by Strickland *et al.* [8] were compared with the PIV data and AFRL force measurements. The comparison between all three measurements is in a good qualitatively and quantitative agreement and it is shown in Figure 8. In Figure 8(a), the highest lift coefficient is recorded at approximately 3.5 between 36° and 45° where the circulation of the LEV starts to grow the fastest. The correlation function reported by Strickland *et al.* [8] shows good agreement with both experimental data sets. An interesting observation is made at low angles of attack where the lift coefficient of approximately 3 is achieved between 18° and 27°. This value of lift coefficient is significantly higher than the steady state value yet the LEV core is not established; this observation is contrary to findings that the LEV must be present in order to generate high lift coefficients beyond static conditions. The inertial effect, or the non-circulatory effects, is a possible explanation for a sudden increase in the lift coefficient, and this becomes more apparent as k is increased to a higher value. As the flat plate rotates to 90°, the lift coefficient decreases to zero while the drag coefficient reaches a value of approximately 4 between 54° and 63°. Discrepancy in the drag coefficient is observed between the 2 experimental data sets and correlation function for geometric angle of attacks beyond 65°. The experimental data sets show decrease in drag coefficient after the peak whereas the correlation function shows a continuous increase as a function of geometric angle of attack.

The error bars in the force coefficients computed from "Flux Equation" is the uncertainty that arise from location of the origin in the computation. The "Flux Equation" requires an origin in the control volume such that the position vector, $\boldsymbol{x}$, can be known. The position vector is then multiplied by the vorticity and the time derivatives in the flow field in order to compute the force coefficients. As the origin is located further from these derivatives, the errors within these derivatives are amplified by the proportional amount. Consequently, the computed force coefficients suffer from these amplified errors and the 95% confidence interval was computed by computing the force coefficients using 30 different origin locations in the control volume.

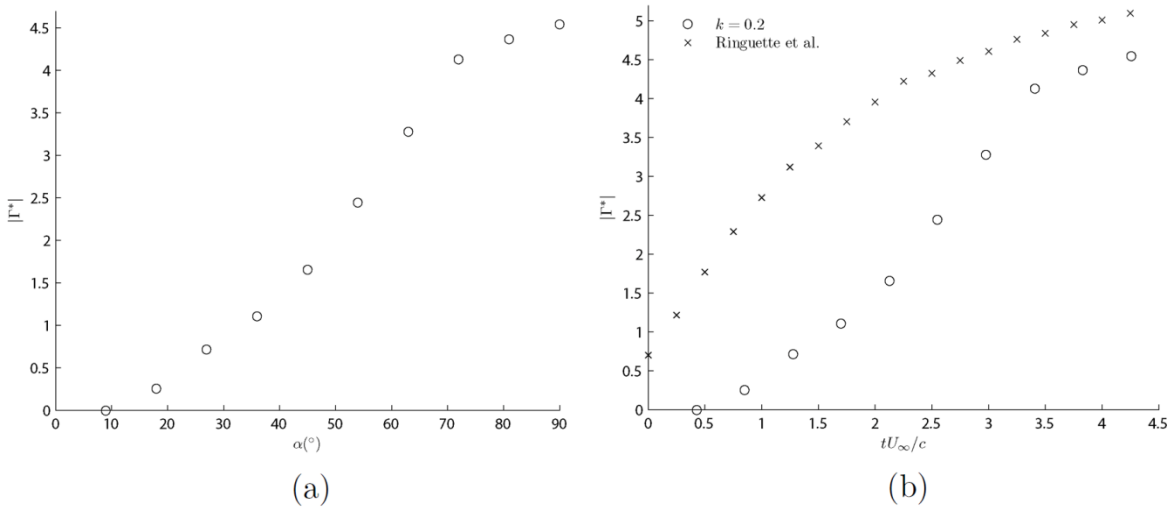

Figure 7. LEV circulation plotted against (a) geometric angle of attack, (b) non-dimensional time for k = 0.20 case.

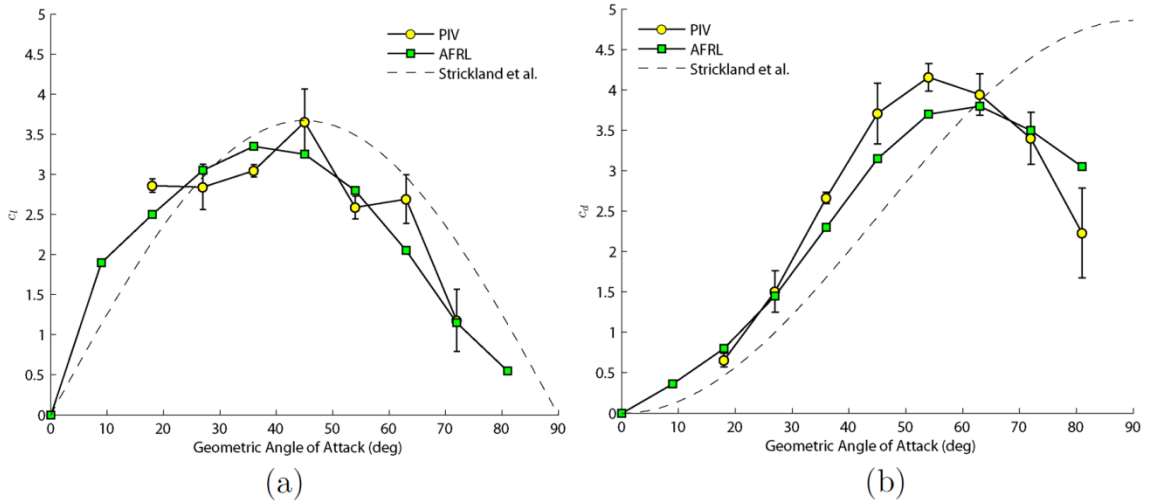

Figure 8. (a) sectional lift coefficient, and (b) sectional drag coefficient computed for k = 0.20 kinematic using "Flux Equation" (PIV), force balance (AFRL), and reported by Strickland *et al.*

B. Results: k = 1.0

A dye injection flow visualization in comparison with the PIV data for k = 1.0 case is shown in Figure 9. The same contour levels, Γ_1, and Γ_2 threshold values used for k = 0.2 case were used. The duration of the pitching motion is approximately 0.935 seconds which is comparable to the convection time, c/U_∞, of 1.08 seconds. The von Karman vortex streets are observed at the wake before the rotation occurs in the Γ_2 contours. Due to the fast pitching maneuver the vortex streets are still captured in the downstream location after 2 convective times after the pitching maneuver. There are several key differences between k = 0.2 and 1.0 cases. Firstly, the high angular velocity of the flat plate induces a strong trailing edge vortex (TEV) at the start. The Γ_1 contours indicate a TEV core at tU_∞/c = 0.18 and it develops in size and strength as it convects downstream. Secondly, the LEV core does not appear until the flat plate has

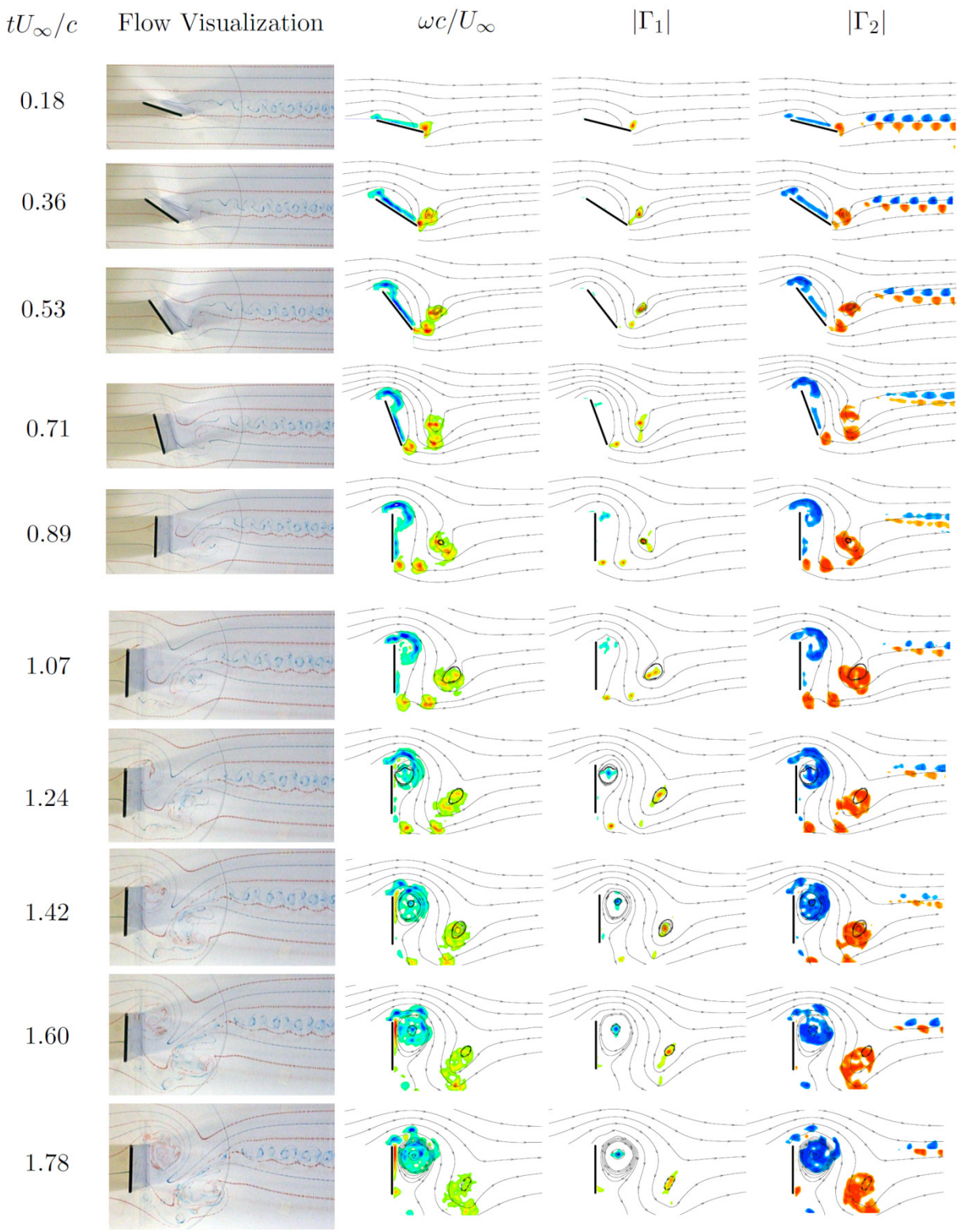

Figure 9. Summary of flow visualization, normalized vorticity, vortex core locations and size for k = 1.0 case.

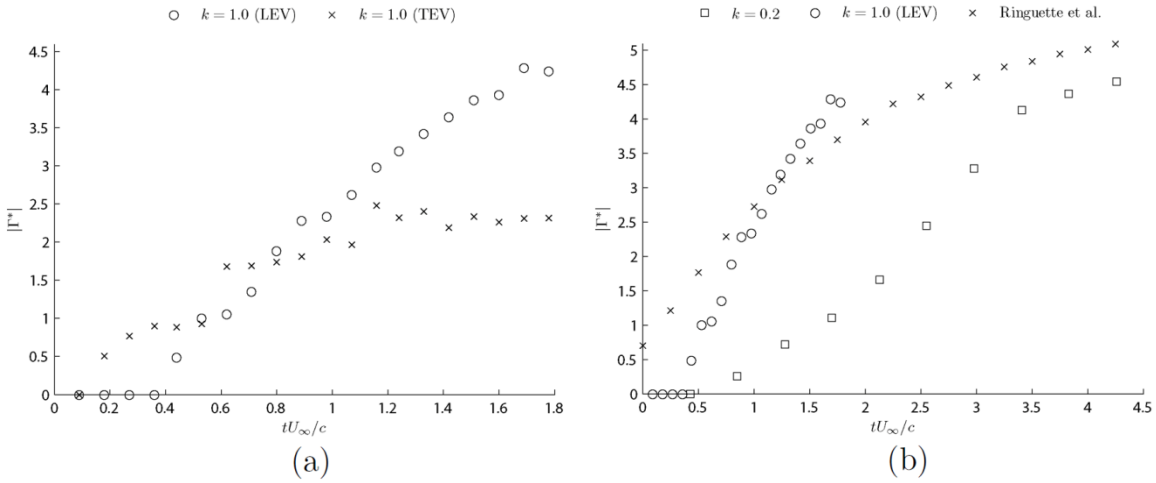

Figure 10. (a) LEV and TEV circulation plotted against non-dimensional time, (b) circulation comparison of k = 0.2 and 1.0, and Ringuette *et al.*

finished its rotation; the first sign of LEV core is shown between tU_∞/c = 1.07 and 1.24 which is well after the flat plate has stopped motion at tU_∞/c = 0.89. However, the Γ_2 contours seem to suggest that there exists a significant part of the flow near the leading edge that is dominated by strong rotation at tU_∞/c = 0.53. The circulation of the leading edge region was computed from tU_∞/c = 0.53 to 1.78, and it is shown in Figure 10.

The normalized circulation values for LEV and TEV are shown in Figure 10(a). TEV circulation experiences 2 jumps in the circulation value at tU_∞/c = 0.6 and 1.1. The rapid increase of TEV circulation at these time intervals is the result of small vortical structures coalescing with the main TEV. The TEV circulation value reaches an equilibrium value at 2.31, which is approximately half of the peak circulation value of 4.3 recorded for LEV circulation. The peak LEV circulation value is obtained one convective time after the motion has stopped while the peak TEV circulation is obtained shortly after the halt of the motion. The flow visualization indicates that the LEV is still developing at tU_∞/c = 1.78, which is equivalent to 2 convective time after the start of the motion. In terms of non-dimensional time, the k = 1.0 case reaches similar LEV circulation value approximately 2.4 times faster than k = 0.2 case. Figure 10(b) compares the LEV circulation value of k = 1.0 case and the impulsively translated flat plate with AR = 6 at 50% span provided by Ringuette *et al*. [12] As discussed earlier, the initial value of LEV circulation is expected to different since the starting conditions are different for both experiments. The flat plate is at 90° geometric angle of attack at tU_∞/c = 0.89 which is the same geometric angle of attack as the impulsively translated flat plate experiment. The key difference is the rate of LEV circulation growth where faster growth rate is reported for the rotated flat plate with the peak value of 4.3 at tU_∞/c = 1.7, and Ringuette *et al.* [12] reports a value of 3.7 at tU_∞/c = 1.7. There are many factors that may contribute to this difference: pivot point location, rotation vs. translation, inertial forces, *Re*, and different AR. The outstanding difference is the AR of the wings where the tip vortex was allowed for form for the AR = 6 and not for the infinite AR wing. The tip vortex may influence the development of the LEV and hence causing discrepancy in the LEV circulation value even at the 50% span location. Another significant difference can be found from the flow topology. The rotating flat plate at k = 1.0 generates a TEV followed by a LEV size that is comparable to the chord length. In the translating flat plate, there are 2 symmetrical vortices that form from both edges of the flat plate. The size and vortex interaction are

inherently different for both cases and this may explain the discrepancies in the LEV circulation values. Nonetheless, it is rather surprising that the LEV circulation values are within the acceptable limit for two different experiments with different parameter and kinematics. It is unclear at the moment whether the normalized LEV circulation value will reach an asymptotic value for both k cases for long convective times.

In relation to the LEV circulation analysis, the force coefficients reveal interesting findings. The force coefficients were computed using the "Flux Equation" from the PIV data set and numerical simulation are shown in Figure 11. The "Flux Equation" shows sign of noise and oscillation in the force coefficients. The error bars indicate 95% confidence interval of force coefficients computed with different origin location. However, the noise and oscillations present in Figure 11 may be due to lack of convergence in the vorticity and time derivative values, in which case acquiring more samples will alleviate this problem. Nonetheless, the qualitative agreement between the "Flux Equation" and CFD force coefficients are acceptable. In addition, force coefficient correlation provided by Strickland *et al.* [8] shows similar qualitative behavior; the correlation function is a function of geometric angle of attack, thus it is symmetric but is incapable of capturing sharp rise in the lift coefficient at the start of the pitching motion. The peak lift coefficient is above 10 and it is approximately 3 times greater than the value reported from k = 0.2 case. The highest lift coefficients are reported between tU_∞/c = 0.18 and 0.71 where the LEV core does not exist. However, there exists a strong TEV that helps the flow to remain attached at high geometric angles of attack. As the flat plate nears 90°, the lift coefficient rapidly drops to zero while the drag coefficient experience a sudden increase. The value of the drag coefficient peaks at approximately 13 for both PIV and CFD. At geometric angle of 90°, the CFD computation reports lift coefficient of zero and drag coefficient that oscillates with mean value of approximately 5. The "Flux Equation" reports lift coefficient that shows oscillatory behavior with mean value approximately zero, while the drag coefficient shows similar trend with mean value of approximately 6. The drag coefficient values are high in both PIV and CFD as the LEV is still developing near the flat plate surface and strong curvature of streamlines indicate an attached LEV. Whether the oscillatory behavior of the drag coefficient will continue for latter convective times is unknown.

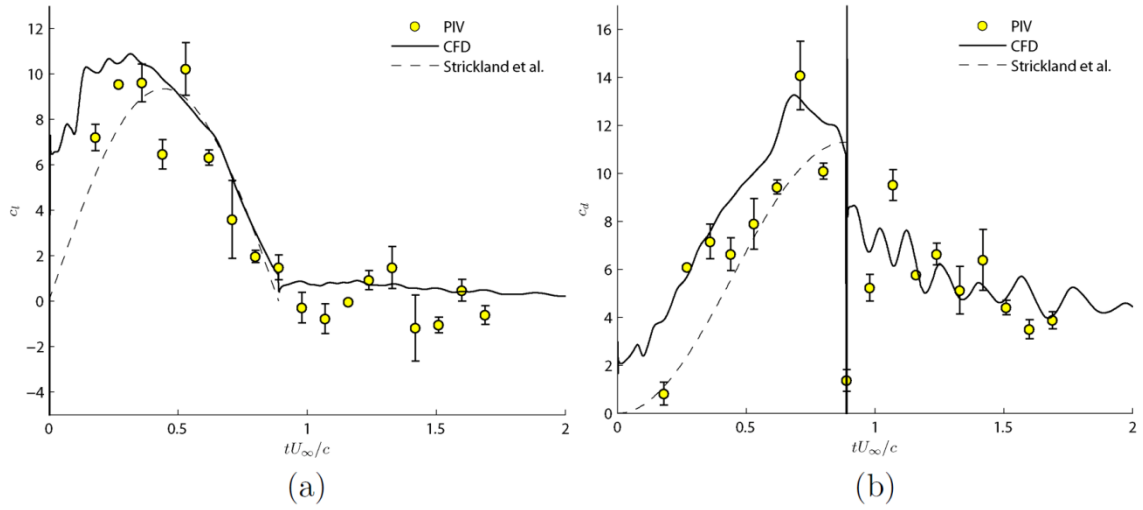

Figure 11. (a) sectional lift coefficient, and (b) sectional drag coefficient computed for k = 1.0 kinematic using "Flux Equation" (PIV), numerical simulation (CFD), and reported by Strickland *et al.*

C. *Return to steady- state*

The pitching motion for k = 0.2 and 1.0 has a convective time of 4.2 and 0.9 respectively. In other words, the flat plate completes the 90° rotation after 4.2 c/U_∞ for k = 0.2 case. Figure 12 summarizes the flow visualization of low and high k cases as a function of convective time. It was observed that k = 1.0 develops LEV core after the flat plate has finished the maneuver. This is shown in Figure 12 where the flat plate is already at 90° geometric angle of attack at 1 c/U_∞. The gradual development of LEV is depicted for k = 0.2 whereas a rapid development of LEV is observed for k = 1.0. For k = 0.2, a pair of vortices are observed at 5 c/U_∞ and the flow resembles a bluff body at 8 c/U_∞. A single large LEV is shown for k = 1.0 and a TEV is formed as the LEV is evinced downstream. The flow visualization comparison between the two cases are different up to 7 c/U_∞; a resemblance in flow topology is found at 7 c/U_∞. The similarity in the flow topology is strengthened in subsequent convective times and the flow field for high k case seems to be a more developed flow field of low k case at 10 c/U_∞. From this observation approximately 7 convective times are required to return the flow in to a steady-state condition for both low and high k cases; higher k case has a delayed LEV formation with respect to the pitching motion but the development with respect to the convective time is increased.

IV. Conclusion

An experimental study of a rapidly pitched flat plate at Re = 5,000 is presented in this paper. The angular amplitude considered is 90° with infinite AR wing that creates a nominally two dimensional flow condition. The reduced frequency of 0.2 and 1.0 are explored with dye flow visualization and 2D PIV. The vortex identification method by Graftieaux *et al.* [15] was implemented to identify the vortex core and its boundary. The LEV circulation analysis was performed and it was compared to the impulsively translating flat plate experiment by Ringuette *et al.* [12] The force coefficients were computed using the "Flux Equation" provided by Noca *et al.* [14] for both low and high k cases. They were compared to the force balance readings from AFRL for k = 0.2 case and numerical simulation for k = 1.0 case. In addition, force coefficient correlations provided by Strickland *et al*. [8] were considered.

The key difference in flow development between low and high k kinematics was the formation of TEV. The low k case developed LEV as the flat plate was performing a rotation. The high k case did not develop LEV core until the flat plate has reached 90° but it developed a strong TEV at the start of the motion. The peak normalized LEV circulation value for both k cases was approximately 4.5 which was slightly less than the value reported for impulsively translated flat plate experiment. While there are many factors that contribute to the difference in both experiments, the discrepancy in the AR seem to influence the flow topology greatly as the tip vortex introduces extrinsic three dimensionality to the flow for low AR wing. Nonetheless, the level of agreement of recorded peak LEV circulation values for rotated and translated flat plate indicate that there may exist a universal threshold circulation value.

The computed force coefficients from the "Flux Equation" resulted in acceptable qualitative comparison with the force balance readings and numerical simulation. In addition, the force correlation provided by Strickland *et al.* [8] was in good quantitative agreement for low k case. For high k case, the qualitative characteristics were present but it was not able to capture a sudden increase in the lift coefficient at the start of the motion. The lift coefficient value exceeding 10 was recorded for high k case which was approximately 3 times greater than low k case. This high lift coefficient value was obtained during the start of the motion where LEV core was not present in the flow field. This was a strong

indication that the inertial, or the non-circulatory effect, was responsible for the high lift generation, not the presence of the LEV. A rapid increase in drag coefficients were observed for both cases as the flat plate reached high geometric angle of attack; the peak drag coefficient was recorded before the geometric angle of attack reached 90°. The PIV data set, AFRL force measurement, and numerical simulation all reported a rapid decrease in drag coefficient value as the flat plate reached closer to 90° geometric angle of attack.

The flow topology between $k = 0.2$ and 1.0 cases was vastly different at the end of the motion due to the fact that the formation time of LEV was delayed for higher k case. However, similarity in the flow topology was observed through dye flow visualization approximately 7 convective times after the start of the motion. After 10 convective times, wake similar to the bluff body condition was observed for both cases which indicated that the flow has reached a steady-state condition.

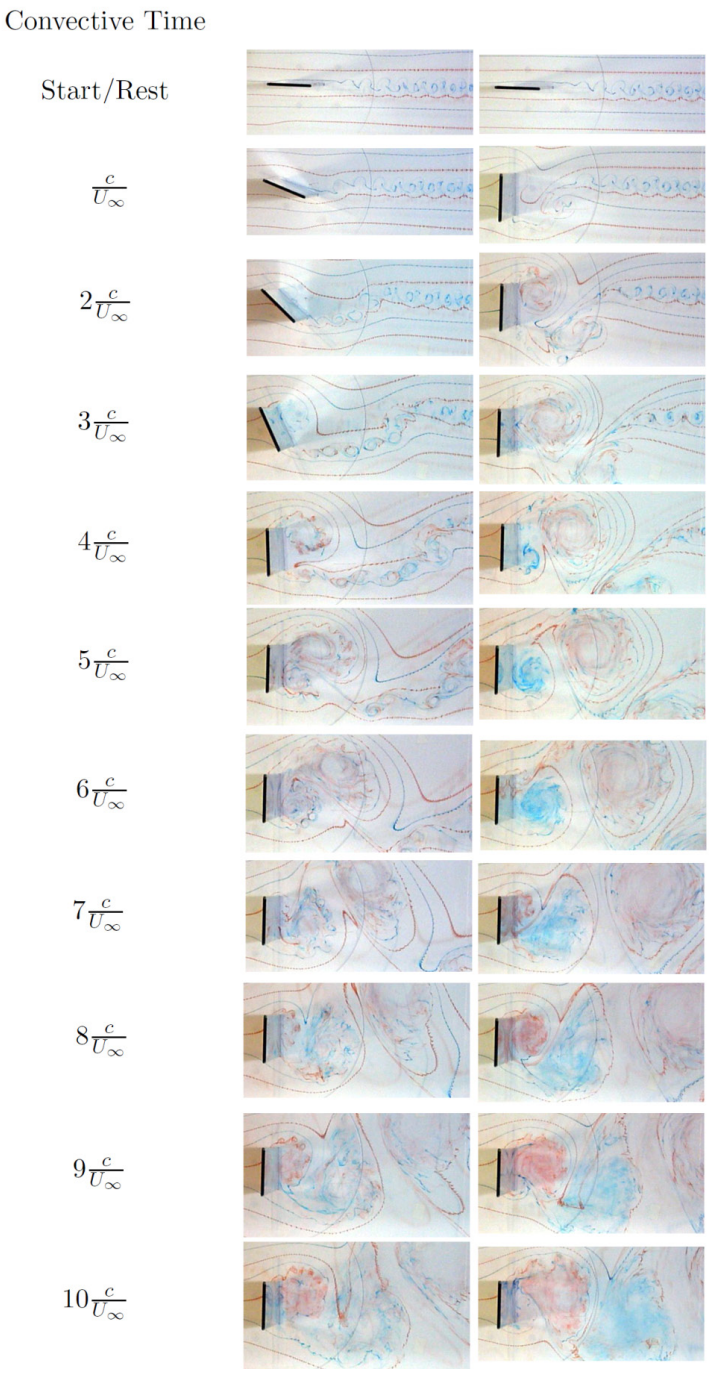

Figure 12. Flow visualization of k = 0.2 and 1.0 cases summarized in convective time scale.

References

[1] Shyy, W., Lian, Y., Tang, J., Viieru, D., & Liu, H. (2008). *Aerodynamics of Low Reynolds Number Flyers.* Cambridge University Press.

[2] Platzer, M., Jones, K., Young, J., & Lai, J. (2008). Flapping Wing Aerodynamics: Progress and Challenges. *AIAA J.* , Vol. 46, No. 9, pp. 2136-2149.

[3] Dickinson, M. H., & Gotz, K. G. (1993). Unsteady aerodynamic performance on model wings at low Reynolds numbers. *J. Exp. Biol* , Vol. 174, pp. 45-64.

[4] Ellington, C. P. (1984). The aerodynamics of hovering insect flight. IV. Aerodynamic mechanisms. *Phil. Trans. R. Soc. Lond. B* , Vol 305, pp. 79-113.

[5] Maxworthy, T. (1979). Experiments on the Weis-Fogh mechanism of lift eneration by insects in hovering flight Part 1. Dynamics of the 'fling'. *J. Fluid Mech.*, Vol. 93, pp. 47-63.

[6] McCroskey, W. J. (1981). The phenomenon of dynamic stall. *NASA TM-81264* .

[7] Walker, J.M., Helin, H.E. & Strickland, J.H. (1985) An experimental investigation of an airfoil undergoing large-amplitude pitching motions, *AIAA J.*, Vol. 23, No. 8, pp. 1141-2.

[8] Strickland, J.H. & Graham, G.M. (1987) Force coefficients for a NACA-0015 airfoil undergoing constant pitch rate motions, *AIAA J.*, Vol. 25, No. 4, pp. 622-4.

[9] Shih, C., Lourenco, L., Van Dommelen, L., & Krothapalli, A. (1992). Unsteady Flow Past an Airfoil Pitching at a Constant Rate. *AIAA J.* , Vol. 30, No. 5, 1153-1161.

[10] Visbal, M. R., & Shang, J. S. (1989). Investigation of the Flow Structure Around a Rapidly Pitching Airfoil. *AIAA J.* , Vol. 27, No.8, 1044-1050.

[11] Reich, G. W., Wojnar, O., & Albertani, R. (2009). Aerodynamic Performance of a Notional Perching MAV Design. *47th AIAA Aerospace Sciences Meeting.* Orlando, FL, AIAA-2009-63.

[12] Ringuette, M., Michelle, M., & Gharib, M. (2007). Role of the tip vortex in the force generation of low-aspect-ratio normal flat plates. J. Fluid Mech, Vol. 581, pp. 453-468,

[13] Ol, M. (2009). The High-Frequency, High-Amplitude Pitch Problem: Airfoils, Plates and Wings. *39th AIAA Fluid Dynamics Conference.* San Antonio, TX, AIAA-2009-3686.

[14] Noca, F., Shiels, D., & Jeon, D. (1999). A Comparison of Methods for Evaluating Time-dependent Fluid Dynamic Forces on Bodies, Using Only Velocity Fields and Their Derivatives. *Journal of Fluids and Structures* , Vol. 13, pp. 551-578.

[15] Graftieaux, L., Michard, M., & Grosjean, N. (2001). Combining PIV, POD and vortex identification algorithms for the study of unsteady turbulent swirling flows. *Measurement Science and Technology,* Vol. 12, pp. 1422-1429

[16] Baik, Y., Rausch, J., Bernal, L. P., & Ol, M. (2010). Experimental Study of Governing Parameters in Pitching and Plunging Airfoil at Low Reynolds Number, *48th AIAA Aerospace Science Meeting.* Orlando, FL, AIAA-2010-388.

[17] Wright, J.A., and Smith, R.W., (2001). "An Edge-Based Method for the Incompressible Navier-Stokes Equations on Polygonal Meshes," Journal of Computational Physics, Vol. 169, pp. 24-43.

[18] Kamakoti, R., and Shyy, W., (2006). "Evaluation of Geometric Conservation Law using Pressure-Based Fluid Solver and Moving Grid Technique", *International Journal of Numerical Methods for Heat & Fluid Flow*, Vol. 14, No. 7, p. 851-865.

[19] Luke, E.A., and George, T., (2005). "Loci: a rule-based framework for parallel multi-disciplinary simulation synthesis," *Journal of Functional Programming*, Vol. 15, Nr. 3, pp.477-502.

[20] Shyy, W., (1985). "A Study of Finite Difference Approximations to Steady-State, Convection-Dominated Flow Problems", *Journal of Computational Physics*, Vol. 57, No. 3, pp. 415-438.

[21] Shyy, W., (1994). *Computational Modeling for Fluid Flow and Interfacial Transport*, Elsevier, Amsterdam.

[22] Blazek, J., (2001). *Computational Fluid Dynamics: Principles and Applications*, Elsevier, Amsterdam.

[23]Thomas, P.D., and Lombard, K., (1978) "The Geometric Conservation Law – A Link between Finite-Difference and Finite-Volume Methods of Flow Computation on Moving Grids", AIAA paper 1978-1208

[24] Balay, S., Buschelman, K., Gropp, W.D., Kaushik, D., Knepley, M.G., McInnes, L.C., Smith, B.F., and Zhang, H, (2009). "PETSc Web page", http://www.mcs.anl.gov/petsc

[25] Kamakoti, R., and Shyy, W., "Evaluation of Geometric Conservation Law using Pressure-Based Fluid Solver and Moving Grid Technique", *International Journal of Numerical Methods for Heat & Fluid Flow*, Vol. 14, No. 7, p. 851-865.

[26] Smith, R.W., and Wright, J.A., (2003). "An Implicit Edge-Based ALE Method for the Incompressible Navier-Stokes Equations," *Int. J. Numer. Meth. Fluids*, Vol 43, pp.253-279

[27] Ho, C., & Huerre, P. (1984). Perturbed Free Shear Layers. *Ann. Rev. Fluid Mech.* , Vol 16, pp. 365-424.

[28] K. Granlund, M.V. Ol, D. Garmann, M. Visbal and L. Bernal, (2010). "Experiments on abstractions of perching" *AIAA 40th Fluid Dynamics Conference and Exhibit*, Chicago, Illinois, AIAA 2010-4943